Faraday Discussions

Cite this: *Faraday Discuss.*, 2017, **200**, 143

PAPER

View Article Online
View Journal | View Issue

# The effect of gas-phase polycyclic aromatic hydrocarbons on the formation and properties of biogenic secondary organic aerosol particles

Alla Zelenyuk,*[a] Dan G. Imre,[b] Jacqueline Wilson,[a] David M. Bell,[a] Kaitlyn J. Suski,[a] Manish Shrivastava,[a] Josef Beránek,[a] M. Lizabeth Alexander,[a] Amber L. Kramer[c] and Staci L. Massey Simonich[cd]

Received 22nd January 2017, Accepted 21st February 2017

DOI: 10.1039/c7fd00032d

When secondary organic aerosol (SOA) particles are formed by ozonolysis in the presence of gas-phase polycyclic aromatic hydrocarbons (PAHs), their formation and properties are significantly different from SOA particles formed without PAHs. For all SOA precursors and all PAHs, discussed in this study, the presence of the gas-phase PAHs during SOA formation significantly affects particle mass loadings, composition, growth, evaporation kinetics, and viscosity. SOA particles formed in the presence of PAHs have, as part of their compositions, trapped unreacted PAHs and products of heterogeneous reactions between PAHs and ozone. Compared to 'pure' SOA particles, these particles exhibit slower evaporation kinetics, have higher fractions of non-volatile components, like oligomers, and higher viscosities, assuring their longer atmospheric lifetimes. In turn, the increased viscosity and decreased volatility provide a shield that protects PAHs from chemical degradation and evaporation, allowing for the long-range transport of these toxic pollutants. The magnitude of the effect of PAHs on SOA formation is surprisingly large. The presence of PAHs during SOA formation increases mass loadings by factors of two to five, and particle number concentrations, in some cases, by more than a factor of 100. Increases in SOA mass, particle number concentrations, and lifetime have important implications to many atmospheric processes related to climate, weather, visibility, and human health, all of which relate to the interactions between biogenic SOA and anthropogenic PAHs. The synergistic relationship between SOA and PAHs presented here are clearly complex and call for future research to elucidate further the underlying processes and their exact atmospheric implications.

---

[a] *Pacific Northwest National Laboratory, USA. E-mail: alla.zelenyuk-imre@pnnl.gov*

[b] *Imre Consulting, USA*

[c] *Department of Chemistry, Oregon State University, USA*

[d] *Environmental and Molecular Toxicology, Oregon State University, USA*

# Introduction

Data from field measurements indicate that a significant fraction of atmospheric SOA mass is formed from biogenic precursors, through pathways that are enhanced by anthropogenic pollution.[1–4] This phenomenon, known as anthropogenic–biogenic interactions, can result in measured SOA loadings that are significantly higher than predicted by models.[5,6] Bateman *et al.*[7] also reported that anthropogenic emissions influence the physical state of submicron organic particles sampled over Amazonia, making them more viscous. Moreover, measurements of the evaporation kinetics of ambient SOA particles, which were shown to be affected by anthropogenic pollution,[1] indicate that they evaporate significantly slower than pure laboratory generated biogenic SOA particles.[8]

Thus far, the laboratory studies attempting to reproduce anthropogenic–biogenic interactions have focused on the effect of acidic sulphate seeds, $NO_x$, and $SO_2$ on SOA formation mechanisms and yields. Anthropogenic pollution includes, in addition to inorganic pollutants, hydrophobic semi-volatile organic compounds, like polycyclic aromatic hydrocarbons (PAHs). PAHs are emitted as byproducts of energy production and consumption, and are extremely toxic.[9] PAHs have been found far from their sources[10–14] and shown to survive much longer in the atmosphere than models predict.[10,15,16]

Our previous studies show that these hydrophobic compounds can adsorb to particle surfaces during secondary organic aerosol (SOA) formation and become entrapped in highly viscous, semi-solid SOA particles.[8,17,18] The limited diffusion of the entrapped PAHs prevents them from evaporating and shields them from oxidation.[17,19] In turn, the presence of PAHs during SOA formation makes these particles less volatile and more viscous.[8,17] The observed synergetic relation between SOA and PAHs, in which SOA provides a protective shield for the PAHs, while the PAHs increase SOA loading, lifetime, and shielding power, enables long-range transport of PAHs inside long-lived atmospheric organic particles by protecting them from the oxidizing atmosphere.[17,19] A recent study also found that, at low RH, the reaction between semi-solid organic particles, composed of shikimic acid, and ozone is limited to the particle surfaces, effectively shielding the particle inner core from oxidation.[20]

The gas-phase reaction rates of PAHs with ozone are orders of magnitude slower than the reactions with OH-radicals,[21] and are therefore usually assumed to play an insignificant role.[22] In contrast, studies have shown that the heterogeneous reactions of PAHs with ozone on surfaces are relatively fast[23–30] and can produce Criegee intermediates,[31–34] which can lead to oligomer formation.[35] Moreover, Miet, *et al.*[33] showed that hydroxypyrene, one of the products of pyrene ozonolysis, was twice as reactive with ozone than pyrene on silica surfaces, indicating that as PAHs are oxidized they could further react with ozone in the particle phase. Similar results were observed for anthracene oxidation products, in a study that found that the reaction led to an increase in particle size with oxidation.[36] This heterogeneous chemistry, if it were to take place on the surfaces of SOA particles, especially as they form, could play an important role in the formation and properties of these particles. All previous studies, however, focused on the reaction between ozone and PAHs in the condensed phase, *e.g.* deposited on particle surfaces, while paying no attention to the presence of PAHs in the gas phase and their potential role in heterogeneous chemistry on particle surfaces.

Here we begin by building on our previous findings to show that the observed interactions between PAHs and SOA particles during formation, which result in slower evaporation, are reproducible for different SOA precursors and different PAHs with a wide range of concentrations. We then examine the differences between 'pure' SOA particles and SOA particles formed in the presence of PAH vapors to show that, while PAHs comprise only a small fraction of the total particle mass, their presence during SOA formation drastically changes particle properties by trapping PAHs and PAH oxidation products, resulting in increased particle viscosity and oligomer content.

We proceed to investigate the heterogeneous ozonolysis of gas-phase PAHs on particle surfaces, using inert ammonium sulfate (AS) particles. These measurements show that the AS particles grew and developed a coating composed of oxidized pyrene products and trapped unreacted pyrene. We show that this organic coating evaporates very slowly and that 70% of its volume is composed of nearly non-volatile compounds.

Finally, we show that the presence of PAHs during SOA formation yields significantly higher SOA mass loadings and particle number concentrations, thereby providing an example of one of the most direct occurrences of the phenomenon known as anthropogenic–biogenic interactions.

# Experimental

Fig. 1 shows a schematic of the experimental setup used to generate, in-parallel, 'pure' SOA particles (upper path) and SOA particles formed in the presence of gas-phase PAHs (bottom path). For clarity, we refer to SOA formed without PAHs as 'pure', even though it is composed of a highly complex mixture of many different

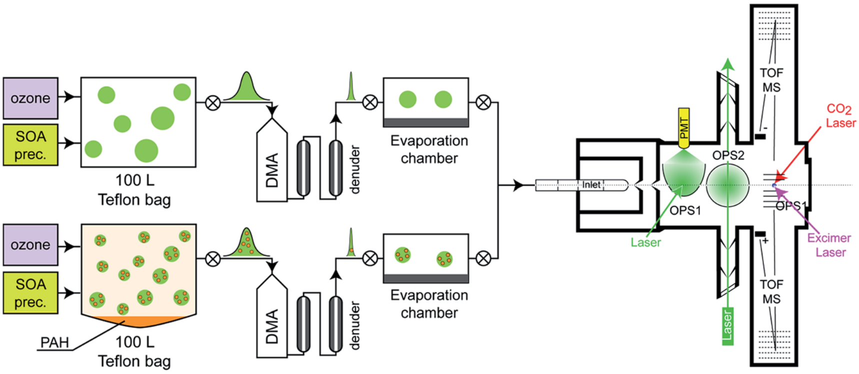

Fig. 1 Schematic of the experimental setup for characterizing particle formation and evaporation kinetics of pure SOA particles (upper path) and SOA particles formed in the presence of PAH vapors (bottom path). Particles are formed by ozonolysis in two parallel pathways, in the 100 L Teflon chambers, and particle formation progress is monitored throughout. Once reaction is complete, particles are size-selected and transferred to the evaporation chambers, through two inline denuders. During evaporation, miniSPLAT or SPLAT II is used to periodically characterize particles size and composition.

components. These parallel experiments were performed on the same day, using new Teflon chambers with SOA formation occurring less than 10 min apart to ensure that even slightly varying laboratory conditions (*e.g.* temperature) would affect both experiments identically. Performing parallel experiments in this manner made it possible to compare the impact PAHs had on SOA formation without taking into account processes such as wall losses.

To generate SOA in the presence of PAH, a small amount (0.1–1 gram) of a single PAH was loaded into the 100 L Teflon reaction chamber at least 24 hours prior to the experiment, and allowed to equilibrate with zero-air. Table 1 lists the seven PAHs that are discussed in this study, their molecular structures, vapor pressures at 25 °C, and the corresponding mixing ratios. Here we will focus mainly on the effect of pyrene (Sigma Aldrich, ≥98%) and benzo(*a*)pyrene (Sigma Aldrich ≥96%).

SOA formation was induced by injecting the SOA precursor, ozone, and ~250 ppm of cyclohexane (Sigma Aldrich, ≥99%), which was used as an OH scavenger, into a 100 L Teflon chamber.[8,37] Seven SOA precursors were used to form pure SOA particles and particles formed in the presence of pyrene: α-pinene,

**Table 1** List of the PAHs discussed in this study, their molecular structures, vapor pressures at 25 °C, and mixing ratios

| Name | Structure | Vapor pressure at 25 °C, Torr | Mixing ratio, ppb |
|---|---|---|---|
| Naphthalene | 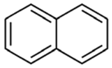 | $7.5 \times 10^{-4}$ | 90 000 |
| Dibenzothiophene | 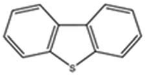 | $2.1 \times 10^{-4}$ | 300 |
| Phenanthrene |  | $1.2 \times 10^{-4}$ | 200 |
| Pyrene | 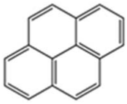 | $4.5 \times 10^{-6}$ | 6 |
| Fluoranthene | 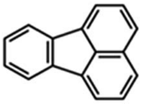 | $9.2 \times 10^{-6}$ | 10 |
| Benzo(*a*)anthracene | 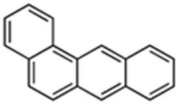 | $2.1 \times 10^{-7}$ | 0.2 |
| Benzo(*a*)pyrene | 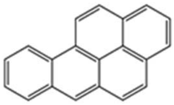 | $5.5 \times 10^{-9}$ | 0.007 |

cyclohexene (Sigma Aldrich, ≥99%), cycloheptene (Sigma Aldrich, ≥97%), cyclooctene (Sigma Aldrich, ≥99.5%), *trans*-3-hexene (Sigma Aldrich, ≥99%), limonene (Sigma Aldrich, ≥96%), and isoprene (Sigma Aldrich, ≥99.5%). All experiments presented here were conducted in excess of ozone (~3× the SOA precursor concentration).

During SOA formation, particle size distributions were periodically monitored using a scanning mobility particle sizer (SMPS, TSI Inc., Model 3936), until SOA formation was complete and particles stopped growing, at which point they were classified with a differential mobility analyzer (DMA, TSI Inc., Model 3081) to generate an aerosol sample with a narrow distribution of mobility diameters. The monodisperse particles were passed through the two inline denuders, and loaded into the evaporation chamber that was partially filled with activated charcoal and kept at room temperature and pressure.[8,17,18] To generate aged particles, the freshly formed particles were left in the reaction chamber for ~24 hours before they were sampled.

Particle shape, vacuum aerodynamic diameter ($d_{\text{va}}$), density, and composition determined from individual particle mass spectra were periodically characterized as a function of evaporation time[8,37–40] using our single particle mass spectrometers, miniSPLAT and/or SPLAT II, described below. The evaporation kinetics data presented here are expressed in terms of volume fraction remaining (VFR), where VFR $\equiv [d_{\text{va}}(t)/d_{\text{va}}(t=0)]$.[3] Typical duration of the evaporation experiments was ~24 hours.[8,17]

To study the reaction between ozone and pyrene on inert surfaces, size-selected ammonium sulfate (AS) particles were introduced into the reaction chamber that was preloaded with pyrene 24 hours prior to addition of AS particles. Once exposed to pyrene vapor, particles were sampled by miniSPLAT to determine whether pyrene adsorbed to the surface of the AS particles. Ozone was then added, and particles were sampled periodically by the SMPS and miniSPLAT to monitor the temporal evolution of particle size and composition with reaction time. Once particles stopped growing, they were loaded into the evaporation chamber and their size and mass spectra characterized by miniSPLAT as a function of evaporation time.

A detailed description of SPLAT II and its miniaturized version, miniSPLAT, their characteristic measurement capabilities, and a complete account of the room-temperature evaporation kinetics experiments are provided elsewhere.[37,39,41,42] Here we provide only a very brief description of the single particle mass spectrometers. An aerodynamic inlet lens is used to generate a collimated particle beam and efficiently transport particles into the vacuum system. Each particle is detected in two optical detection stages, and the measured particle time-of-flight between the two stages is used to calculate particle velocity yielding particle vacuum aerodynamic diameter ($d_{\text{va}}$) with better than 0.5% precision and accuracy. The two optical detection events are also used to generate triggers to pulsed infra-red (IR) and ultra-violet (UV) excimer lasers. The IR $CO_2$ laser (GAM Lasers, Model EX5/200, 9.4 μm) is used to evaporate the semi-volatile fraction of each particle and the time-delayed UV excimer laser (GAM Lasers, Model EX5/300, 193 nm) is used to ionize the molecules in the expanding plume of evaporating gas and ablate the non-volatile fraction. The two-step ion generation scheme was shown to significantly improve the instrument quantitative capabilities.[39,41,43] In SPLAT II ions are detected and analyzed with an angular reflectron time-of-flight mass spectrometer (TOF-MS, R. M. Jordan, Inc., Model D-850), while miniSPLAT uses a dual-polarity *Z*-configuration reflectron time-of-flight (Z-TOF) mass spectrometer.[41,42] Each mass spectrum presented here represents an average of 1000–2000 individual particle mass spectra. Moreover, the line-shape and position of the $d_{va}$ distribution of monodisperse particles are used to determine particle shape (sphericity/asphericity) and density, with high precision, with spherical particles having narrow line-shape and aspherical particles exhibiting broad $d_{va}$ size distributions.[37]

In two experiments (pure α-pinene SOA particles and SOA formed in the presence of pyrene) an Aerodyne high-resolution time-of-flight mass spectrometer (HR-ToF-AMS)[44] was used to obtain mass spectra of polydisperse particles.

## Results and discussion

The following section will present and discuss a series of experiments designed to elucidate the interactions between PAHs and SOA formed from ozonolysis of biogenic and model precursors. As mentioned above, gas-phase reactions of PAHs with ozone are very slow, rendering them an insignificant source of SOA. Nevertheless, we have shown that when PAHs are present in the gas phase during SOA formation by ozonolysis, the composition and the properties of the resultant SOA particles (*e.g.* density, evaporation kinetics, viscosity, and diffusivity) are different from pure SOA particles formed under identical conditions.[8,17,18] The same study also showed that when pure SOA is formed and subsequently coated with pyrene, by condensation of supersaturated gas-phase pyrene, a nodule of pyrene forms on the surface of the SOA particle, creating an aspherical particle, in which pyrene does not mix with the underlying pure SOA seed.[17,18] When placed in the evaporation chamber, the pyrene nodule readily evaporates and the composition and properties of the underlying SOA particle are unchanged, which demonstrates that pyrene itself does not diffuse into the SOA particle and that PAHs need to be present during SOA formation to impact SOA properties.[17,18]

We begin by comparing pure α-pinene ozonolysis SOA (αP-SOA) and α-pinene SOA formed by ozonolysis in the presence pyrene vapor (αP-PY-SOA), whose concentration is estimated to be 6 ppb or slightly less (Table 1). In both cases, the formed particles were spherical.[17,18] The density of αP-PY-SOA was 1.27 ± 0.02 g cm$^3$, which is higher than density of pure αP-SOA particles (1.18 ± 0.02 g cm$^3$), indicating a significant change in particle properties and composition.[17,18]

Fig. 2a shows a comparison between the evaporation kinetics of size-selected αP-SOA and αP-PY-SOA for both fresh and aged particles. As a reminder, aged particles are those left in the reaction chamber at room temperature for ~24 hours, before being transferred into the evaporation chamber (Fig. 1). No ozone was added during the aging process and the gas-phase concentration of pyrene remained constant, assured by the presence of bulk pyrene in the reaction chamber. In all cases, the evaporation kinetics were measured on mobility-selected particles, which yielded easily resolvable data for two particle sizes that correspond to singly- and doubly-charged SOA particles. Changes in particle size and composition, as a function of evaporation time, were measured with either SPLAT II or miniSPLAT, both of which have high sensitivity, making it possible to follow the evaporation for many hours.[8,41,42]

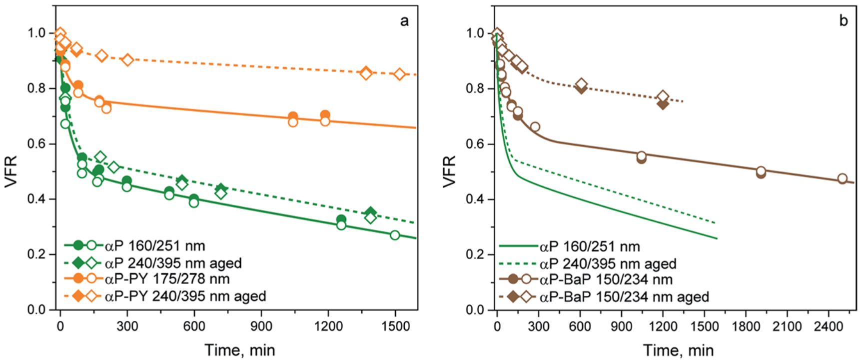

Fig. 2 (a) Measured evaporation kinetics of fresh and aged 'pure' α-pinene SOA particles (αP, green) and SOA particles formed in the presence of pyrene (αP-PY, orange), with the two particle sizes for each experiment indicated; (b) measured evaporation kinetics of fresh and aged 'pure' αP-SOA particles (copied from (a)) and SOA particles formed in the presence of benzo(*a*)pyrene (αP-BaP, brown).

The four evaporation kinetics curves in Fig. 2a, plotted as volume fraction remaining (VFR) *vs.* time, are clearly different. However, the general shape of the curves is similar. Overall, the early stage of evaporation (0–120 min) is relatively fast, with subsequent evaporation slowing with time. This general trend in evaporation kinetics has been reproducible for all SOA particles investigated thus far.[8,17,18,45] The evaporation timescale in Fig. 2a extends beyond 24 hours, yet in all four cases, a significant fraction of the particle volume remains. The most obvious differences between the evaporation kinetics in Fig. 2a, and in general between all SOA systems, is the VFR after long evaporation times (∼24 hours), which for simplicity will be referred to as the asymptotic VFR.

Another feature, common to the evaporation of all SOA particles, under all conditions, including high RH,[45] is that the evaporation kinetics are nearly particle size-independent.[8,17,18,45] This nearly size-independent evaporation is inconsistent with the evaporation kinetics predicted for particles with low-viscosity, where small particles are supposed to evaporate relatively faster than large particles.[8,46,47]

The evaporation of αP-SOA, shown in Fig. 2a, exhibits the typical behavior with an asymptotic VFR of ∼25%, which is consistent with previous measurements.[8,17,45] By comparison, the evaporation of αP-PY-SOA is significantly slower, such that after ∼24 hours of evaporation the asymptotic VFR is 70%. The decrease in evaporation rate has important atmospheric implications: it demonstrates that, as an air mass advects and dilutes, a large volume fraction of the SOA particles remains in the condensed phase. Moreover, the decrease in the rate of particle evaporation would also affect the atmospheric evolution of the PAHs that are trapped in these particles. This symbiotic relationship, in which the presence of PAHs during SOA formation yields longer-lived SOA particles, in turn providing protection for trapped PAHs from the oxidizing atmosphere, enables long-range transport of these toxic compounds.[17,19]

The mass spectra of αP-PY-SOA particles shows a parent ion peak for pyrene molecules ($m/z$ = 202), which we have used to follow the diffusion and evaporation of pyrene from these particles.[18] This analysis indicates that it takes ∼24 hours for about half the pyrene to diffuse from the SOA particles and evaporate.[8,18] In contrast, pyrene deposited on the surface of pure αP-SOA particle evaporates in minutes, leaving no detectable trace behind, and the remaining SOA particle evaporates at the same rate as pure SOA.[18] These results suggest that pyrene can significantly affect the properties of SOA particles, when present during particle formation.

The dashed lines in Fig. 2a present the evaporation kinetics of aged SOA particles, showing that the evaporation of aged αP-SOA particles is only slightly slower and the asymptotic VFR is only ∼5% higher than that for fresh αP-SOA. By comparison, for αP-PY-SOA, aging results in an increase of the asymptotic VFR from ∼70% to 83%. Measurement of diffusion and evaporation of pyrene from inside the aged αP-PY-SOA particles shows it to be slower by a factor of three, indicating particles harden with time.[18] Note that the asymptotic VFR is an approximate measure of the nearly non-volatile content of these particles, the composition of which includes extremely low volatility organic components (ELVOC or highly oxidized molecules (HOM)) that form in the gas phase[48,49] and oligomers that form in the condensed phase.[46,50–56] The formation of the latter has been demonstrated here by the significant increase in the asymptotic VFR with the addition of pyrene and with aging. Comparison between the four curves in Fig. 2a indicates that the fraction of nearly non-volatile molecules in particles formed in the presence of pyrene is more than a factor of two higher that in 'pure' SOA. Similarly, the increase in the asymptotic VFR for αP-PY-SOA with aging suggests that particle-phase oligomer formation continues during aging and impacts αP-PY-SOA more than αP-SOA. Moreover, Fig. 2a shows that the rates of VFR decrease at long evaporation times (>100 min) and that the evaporation rate of αP-PY-SOA is five times slower than that of αP-SOA. If we presume that the very slow evaporation at long times (>100 min) reflects the rate of oligomer decomposition in the particle phase,[55,57] then these data would suggest that the oligomers in αP-PY-SOA are more strongly bound than their αP-SOA counterparts. Overall, the data indicate that aging of αP-PY-SOA increases particle oligomer content and, as was previously shown, increases particle viscosity by ∼a factor of 3.[18] These findings reveal a simple correlation between particle oligomer content and its viscosity, consistent with measurements conducted on polymer-containing systems.[58]

The obvious question is whether the large effect observed with pyrene is due to its relatively high equilibrium vapor pressure at room temperature (Table 1) and whether at lower concentrations, representative of ambient conditions, no effects would be detectable. Because it is difficult to control the concentrations of PAHs below their equilibrium vapor pressures due to wall losses, benzo(*a*)pyrene (BaP) was used instead. The equilibrium vapor pressure of BaP at 25 °C is $5.5\ 10^{-9}$ Torr, which corresponds to a mixing ratio in the reaction chamber of 7 ppt or less, nearly 1000 times lower compared to pyrene.

α-Pinene SOA particles formed in the presence of benzo(*a*)pyrene (αP-BaP-SOA) are spherical and have an initial density of 1.21 ± 0.01 g $cm^3$, and 1.23 ± 0.02 g $cm^3$ after aging for 24 hours. The evaporation kinetics for αP-BaP-SOA and αP-SOA are shown for comparison in Fig. 2b. The observed asymptotic VFR for αP-BaP-SOA of 50% demonstrates that, similar to pyrene, the presence of BaP during SOA formation results in particles that evaporate slower than pure αP-SOA. The figure also shows that aged αP-BaP-SOA evaporates even slower and the asymptotic VFR increases to 75%.

Similar experiments with α-pinene were performed using the seven different PAHs listed in Table 1, with concentrations between 7 ppt to 100 ppm, all showing similar effects.[17] All of the evaporation curves have asymptotic VFR between 50%, for benzo(*a*)pyrene, and 75%, for pyrene, and, in all cases, aging leads to significantly higher asymptotic VFR. Interestingly, the changes in SOA evaporation kinetics were not quantitatively related to the PAHs vapor pressure. For example, naphthalene, whose concentration in the reaction chamber was ~100 ppm, has a smaller effect than pyrene, whose concentration was ~6 ppb.

Thus far, the data show that the presence of gas-phase PAHs during α-pinene SOA formation significantly affects particle properties, reducing their evaporation rates and increasing their oligomer content. Below we will show that this behavior is reproducible for other SOA precursors.

Fig. 3a–d show measured evaporation kinetics of fresh and aged size-selected SOA particles formed by ozonolysis of four different precursors, pure and in the presence of pyrene. In all cases the plots display the evaporation kinetics for two particles sizes: the data for smaller particles are denoted using solid symbols, while larger particles, selected by the DMA as doubly-charged, are shown as open

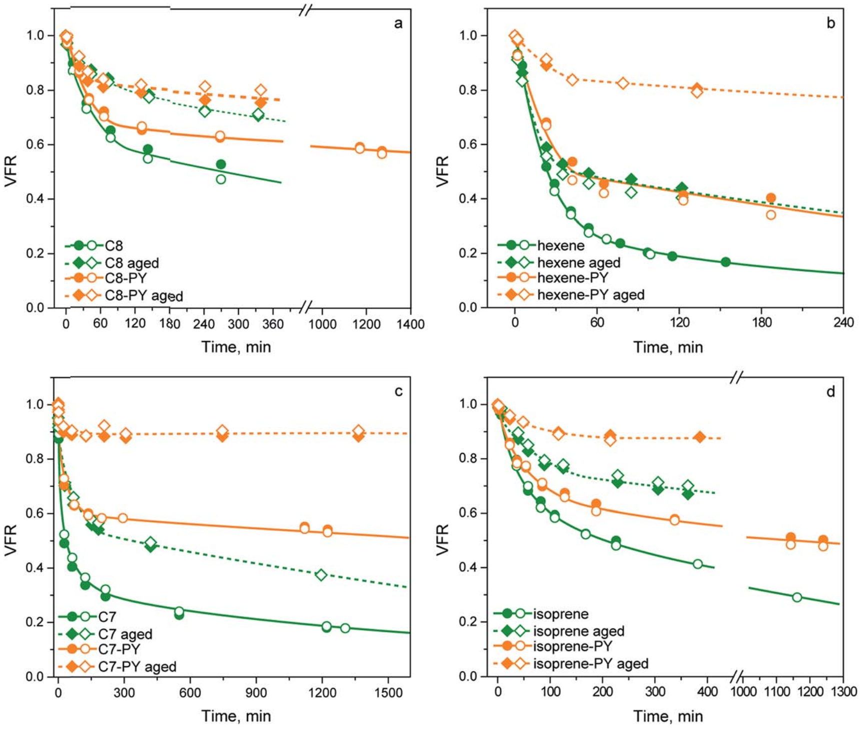

Fig. 3 Measured evaporation kinetics of fresh and aged 'pure' SOA particles (green) and SOA particles formed in the presence of pyrene (orange), for four different precursors: (a) cyclooctene (C8, C8-PY); (b) *trans*-3-hexene SOA particles (hexene, hexane-PY); (c) cycloheptene (C7, C7-PY); and (d) isoprene (isoprene, isoprene-PY).

symbols. Fig. 3a shows that the evaporation kinetics of fresh, pure cyclooctene SOA particles (C8-SOA), whose density is 1.21 ± 0.02 g cm$^{-3}$, are very similar to αP-SOA. Aged cyclooctene SOA evaporated slower, such that after 300 minutes the VFR is 75%. The density of cyclooctene SOA particles formed in the presence of pyrene (C8-PY-SOA) is higher (1.26 ± 0.02 g cm$^{-3}$) and their evaporation is slower than that of pure C8-SOA particles. Similar to other SOA systems, aging increases the asymptotic VFR, *i.e.* increases SOA oligomer content.

Fig. 3b shows the evaporation kinetics of *trans*-3-hexene SOA particles. Pure hexene-SOA particles have a density of 1.15 ± 0.02 g cm$^{-3}$ and evaporate faster than αP-SOA, with VFRs dropping below 20% after 150 min. Aging these particles significantly decreases their evaporation rate, increasing the asymptotic VFR by nearly 30%. *trans*-3-Hexene SOA particles formed in the presence of pyrene, have a density of 1.27 ± 0.02 g cm$^{-3}$ and evaporate significantly slower than pure particles. Fresh hexene-PY-SOA particles have VFR of 45% after 150 minutes of evaporation, while the VFR for aged particles is ~83% after 150 minutes of evaporation.

The analogous data for cycloheptene SOA particles are presented in Fig. 3c. Pure cycloheptene SOA particles (C7-SOA) have a density of 1.21 ± 0.02 g cm$^{-3}$ and an asymptotic VFR of ~20% after ~20 hours of evaporation. By comparison, aged (C7-SOA) particles have an asymptotic VFR of ~40% over a similar evaporation time scale. As before, cycloheptene SOA particles formed in the presence of pyrene (C7-PY-SOA) evaporate significantly slower and have asymptotic VFR of 55% and 80% after ~20 hours of evaporation for fresh and aged particles, respectively.

In addition to the last three model SOA systems, Fig. 3d shows the evaporation kinetics for SOA formed from isoprene, another important biogenic SOA precursor. Even though isoprene SOA typically forms from OH photochemistry, recent studies have suggested that ozonolysis of isoprene could also be a source of atmospherically relevant SOA.[59,60] The evaporation data for isoprene SOA (Fig. 3d) exhibit patterns very similar to those shown in Fig. 3a–c. Fresh and aged pure isoprene SOA evaporation kinetics have asymptotic VFR of ~25% and ~60%, respectively, after ~20 hours of evaporation. Isoprene SOA formed in the presence of pyrene evaporate slower, with asymptotic VFR of 45% and 80% for fresh and aged particles, respectively.

The data presented in Fig. 2 and 3 have demonstrated a reproducible trend in the way the presence of PAHs and particle aging affect the evaporation kinetics of SOA particles formed by ozonolysis. We find, however, that limonene, another biogenic SOA precursor, exhibits a slightly different behavior. Under our experimental conditions, limonene ozonolysis produces a large number of SOA particles at a rate much faster than that observed for all the other precursors discussed here. The data show that the evaporation of limonene SOA particles formed with or without pyrene present, is nearly the same. However, the evaporation kinetics of aged particles, formed in the presence of pyrene, are significantly slower than those for pure aged limonene SOA particles. Examination of the mass spectra of limonene SOA formed in the presence of pyrene reveals that only a small amount of pyrene is present.

To understand better the effect of PAHs on SOA, we first examine the SPLAT II mass spectra of SOA particles formed in the presence of pyrene. In our single particle mass spectrometers individual particle mass spectra can be generated by ablation with the UV excimer laser or using a two-step IR/UV process, which uses a pulse from the $CO_2$ laser to heat the particle and evaporate the semi-volatile fraction, followed by a time-delayed excimer laser pulse that ionizes the evaporated fraction, in the gas phase, and ablates the non-volatile fraction that remained in the particle.[41,43] Previously it has been shown that gas-phase ionization of semi-volatile compounds desorbed/evaporated from the particle produces more ions than ablation.[39,41,43] The differences between mass spectra obtained by laser ablation and by the two-step IR/UV process can, therefore, be used to distinguish between peaks in the mass spectra associated with the semi-volatile and non-volatile fractions present in the particle.[39,41]

Fig. 4 shows the results of such an experiment on fresh cycloheptene SOA formed in the presence of pyrene. The mass spectrum marked in violet was generated by ablation and the two-step process generated the mass spectrum marked in red. The figure shows that, at low $m/z$, the intensity of the peaks generated by the two-step process is significantly higher than that generated by ablation only, as has been observed for semi-volatile molecules.[39,41,43] In contrast, the intensities of the peaks at the high $m/z$ region of the two mass spectra are virtually the same, indicating that these mass spectral peaks represent nearly non-volatile molecules, like oligomers. Note that while there is a significant difference between the two spectra in the intensity of the pyrene parent ion peak at $m/z = 202$, the intensity of the peak at $m/z = 205$ is the same in both mass spectra. Several studies identified the mass spectral fragment at $m/z = 205$ ($C_{15}H_9O^+$) as a marker for products of pyrene heterogeneous reaction with ozone.[31–33,61,62] The data shown in Fig. 4 indicate that, when pyrene gas-phase molecules are present during SOA formation, they contribute to the particle growth in two ways. During particle growth, pyrene adsorbs to the particle surface and becomes trapped/

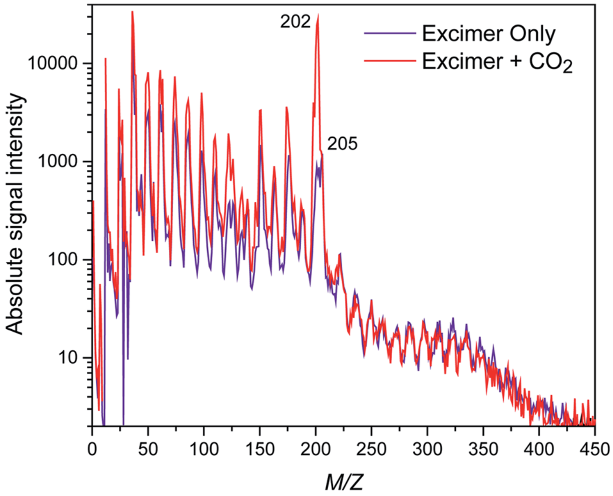

**Fig. 4** Two superimposed SPLAT II mass spectra of fresh cycloheptene SOA formed in the presence of pyrene, which were generated by ablation with the excimer laser (violet) and in a two-step process, using the $CO_2$ laser to evaporate the semi-volatile components and the delayed excimer laser to ionize the evaporated molecules in the gas phase and ablate those remaining in particle phase (red).

buried under condensing SOA, leading to the signal at $m/z = 202$. In addition, pyrene undergoes heterogeneous chemistry with ozone to increase particle mass and enhance the formation of low-volatility products, resulting in the observed peak at $m/z = 205$ and other high $m/z$ peaks.

The high UV laser ionization efficiency of PAHs, compared to other hydrocarbons like SOA, makes it nearly impossible to quantify the relative amount of PAHs in the particles from the mass spectra acquired by SPLAT II. To estimate the relative amount of pyrene present in αP-PY-SOA particles we use the Aerodyne high resolution time-of-flight aerosol mass spectrometer (HR-ToF-AMS)[44] to obtain mass spectra of αP-SOA and αP-PY-SOA particles. Fig. 5a shows two superimposed HR-ToF-AMS mass spectra of aged αP-SOA and αP-PY-SOA particles, sampled directly from the Teflon chambers. It shows that at low $m/z$, the mass spectra have nearly the same peak intensities, and that the intensities above $m/z = 170$ are nearly all due to αP-PY-SOA particles. In addition to the unreacted pyrene parent ion peak ($m/z = 202$), other mass spectral peaks (labeled in Fig. 5a) are clearly observable. Some of the prominent peaks were assigned to the known products of heterogeneous chemistry between ozone and pyrene,[32] *e.g.* hydroxypyrene ($C_{16}H_{10}O$, $m/z = 218$), 4-carboxy-5-phenanthrene-carboxyaldehyde ($C_{16}H_{10}O_3$, $m/z = 250$ and its fragment at $m/z = 205$). From these mass spectra, we estimate the fraction of pyrene and its ozonolysis products in these SOA particles to be ~5%. Fig. 5b presents the same mass spectra, but on a log scale, illustrating that the mass spectrum of aged αP-PY SOA particles exhibits increased relative intensity of peaks at high $m/z$, suggesting they have higher oligomer content, which is in agreement with the particle evaporation data shown in Fig. 2a.

Fig. 6a and b illustrate the temporal evolution of the relative mass spectra peak intensities as a function of evaporation time for aged C8-PY-SOA, focusing on the pyrene parent ion peak ($m/z = 202$), the peak at $m/z = 205$, and the higher $m/z$ peaks. Fig. 6a shows a systematic decrease in the relative mass spectral intensity of the pyrene parent ion peak with evaporation, which is due to the diffusion of semi-volatile pyrene through the SOA particle and its eventual evaporation. As previously shown,[18] the observed changes in pyrene peak intensity as a function of

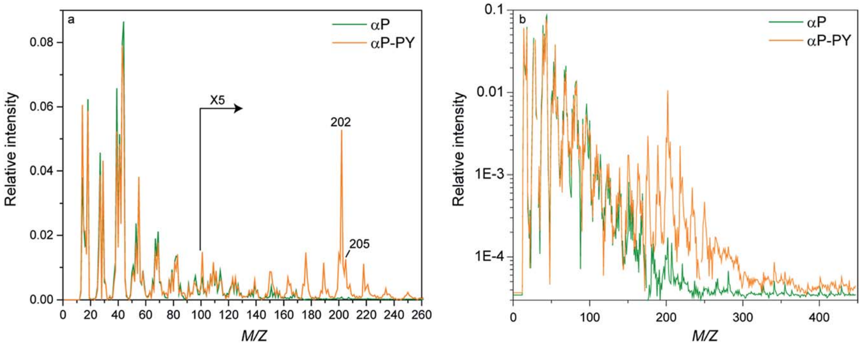

Fig. 5 Two superimposed HR-ToF-AMS mass spectra of aged 'pure' α-pinene SOA particles (αP, green) and SOA particles formed in the presence of pyrene (αP-PY, orange) with relative mass spectral intensities shown on linear (a) and logarithmic (b) scales.

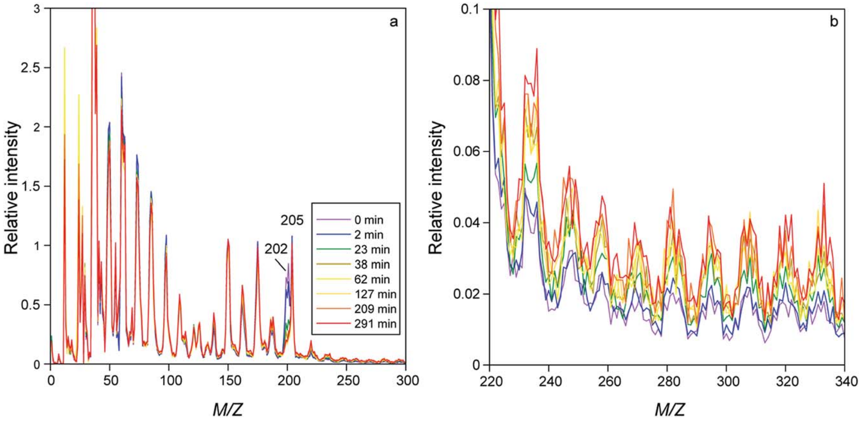

Fig. 6 Superimposed mass spectra of aged cyclooctene SOA particles formed in the presence of pyrene as a function of the evaporation times indicated in the legend. (a) Overview of changes in the relative peak intensities; (b) an expanded scale of the higher *m*/*z* of the mass spectra shown in (a).

evaporation time can be used to calculate its chemical diffusivity in SOA particles and estimate particle viscosity. For aged C8-PY-SOA particles this approach yields pyrene diffusivity of $D = 5 \times 10^{-20}$ m$^2$ s$^{-1}$ and viscosity of $\eta = 2 \times 10^7$ Pa s, indicating that at low RH these particles are semi-solids. Fig. 6a also shows that the relative intensity of the peak at $m/z = 205$ does not decrease with evaporation time, indicating that it represents a fragment of a low-volatility compound, in agreement with data presented in Fig. 4. Similarly, we find that the relative intensity of the mass spectral peaks at higher *m*/*z* increases with evaporation time, which is demonstrated in Fig. 6b, in an expanded scale. This trend, shown here for aged C8-PY-SOA, is consistent with our previously reported behavior for αP-PY-SOA particles.[8]

All of the experiments described thus far were conducted under dry conditions. Given that atmospherically relevant RH is significantly higher and that at elevated RH the viscosity of SOA particles was shown to decrease,[63,64] the atmospheric relevance of these findings could be questioned. Preliminary experiments conducted with αP-PY-SOA and αP-SOA show that, even at 90% RH, the difference between the two remains, with αP-PY-SOA particles having an asymptotic VFR of 55%, as compared to a VFR of 20% observed for αP-SOA.[45] These results demonstrate that the effect of pyrene on the evaporation of SOA particles persists even at high RH. Fig. 7 shows an expanded scale of the mass spectra of αP-PY-SOA particles formed in the presence of pyrene under dry conditions and evaporated for 190 minutes at low (<5%) RH (red) and at 90% RH (blue). All the peaks in the two superimposed mass spectra are nearly identical, except for the pyrene parent ion peak at $m/z = 202$, which has lower intensity at high RH. This difference reflects the fact that the particle viscosity at 90% RH is lower than at dry conditions,[63] leading to higher pyrene diffusivity and hence its faster evaporation.

It is important to point out that all studies described here were conducted at room temperature and that the atmospheric temperature varies significantly. This is particularly important for long-range transport of PAHs that could be taking

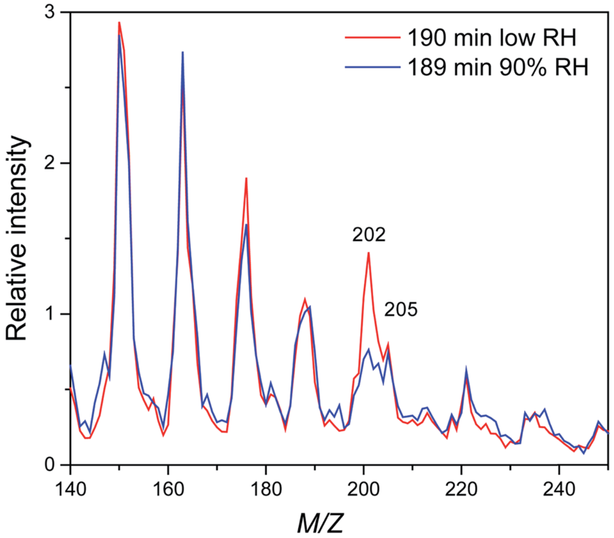

Fig. 7 Comparison between the mass spectra of α-pinene SOA particles formed in the presence of pyrene (αP-PY-SOA) and evaporated for 190 minutes at low RH (red) and at 90% RH (blue).

place at much lower temperatures,[19] for which one would expect slower evaporation rates and higher viscosity.[20,65]

It is clear that the magnitudes of the PAH effect on SOA evaporation kinetics and oligomer content vary somewhat, depending on the PAH, the SOA precursor, the RH, and temperature. Nevertheless, the effects are significant, and their overall pattern is reproducible. It is worth noting that, although very limited, measurements of the evaporation kinetics of ambient atmospheric SOA particles at room temperature show that their asymptotic VFRs are between 80% to 90%,[8] which as the data presented here show, is similar to that seen for aged SOA particles that were formed in the presence of PAHs.[8]

The mass spectra presented above show that SOA particles formed by ozonolysis in the presence of gas-phase pyrene contain some trapped pyrene and known pyrene heterogeneous ozonolysis products. Moreover, the evaporation studies demonstrate that both pyrene and its ozonolysis products remain in the particles for over 24 hours. This proves that the influence of PAHs is not limited to the particle surface, and thus confirms that ozonolysis of PAHs occurs throughout aerosol formation and growth, allowing these products (and unreacted PAHs) to become incorporated inside the SOA particles.

Below we describe a study on a somewhat simplified system, designed to gain insight into the reactions between PAHs and ozone on the surface of SOA particles during SOA formation. Size-selected ammonium sulfate (AS) particles were used to provide an inert surface for the reaction between pyrene and ozone. The mass spectra of pure AS particles, AS particles exposed to gas-phase pyrene, and AS particles after addition of ozone are presented in Fig. 8a. The figure shows that before AS particles were introduced into the reaction chamber they contained no organics. Once introduced into the reaction chamber saturated with pyrene

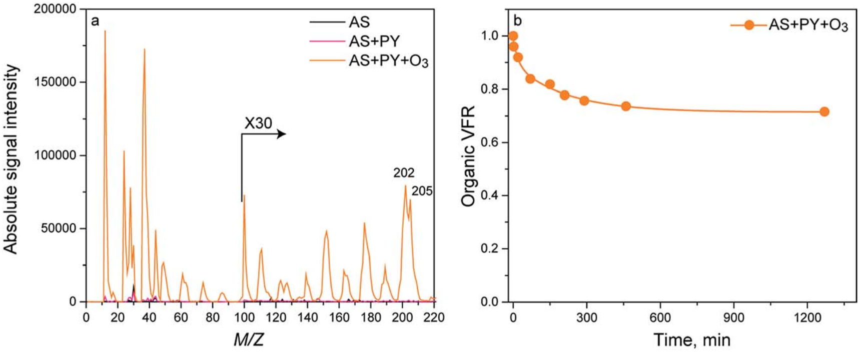

**Fig. 8** (a) Three superimposed mass spectra of 'pure' ammonium sulfate (AS) particles, AS particles exposed to gas-phase pyrene (AS + PY), and AS particles an hour after ozone was added (AS + PY + $O_3$); (b) evaporation kinetics of the organic coating formed on the AS particles.

vapor, the particle mass spectra show adsorbed pyrene. No changes in particle size are observed at this point. Following the introduction of ozone into the chamber, within an hour particle $d_m$ increased from 150 nm to 168 nm, which together with the dynamic shape factor of AS can be used to calculate a thickness of ~10 nm for the organic coating. The mass spectrum of the coated AS particles, shown in Fig. 8a, exhibits familiar peaks at $m/z = 202$ and $m/z = 205$ for pyrene and pyrene reaction products, respectively, as observed for SOA particles formed in the presence of pyrene.

Similar to all of the SOA systems discussed above, the evaporation kinetics of the coated AS particles were characterized using miniSPLAT to measure changes in particle $d_{va}$ with evaporation time. For these mixed particles it is essential to know the density of the organic layer to convert changes in $d_{va}$ to the changes in the VFR of the organic layer. The fact that we used $d_m$-selected AS seed particles makes it possible to account for the contribution of the AS seed to the particle density measurement to obtain a density of $1.25 \text{ g} \pm 0.02 \text{ cm}^{-3}$ for the organic layer. The contribution of the inert seed is also taken into account to calculate the evaporation kinetics for the organic layer only, which is shown in Fig. 8b. The figure shows that the evaporation kinetics of this organic layer are very slow and ~70% of its volume is composed of nearly non-volatile compounds.

Most interestingly, the mass-spectral data analysis indicates that the relative intensities of peaks at $m/z = 202$ and $m/z = 205$ remain nearly constant during evaporation of this organic layer, suggesting that, unlike pyrene diffusion in SOA particles, pyrene diffusion through the organic layer formed on the AS seeds is insignificant.

This experiment with an inert seed clearly shows that, on the time scales commonly used for SOA formation experiments, pyrene reacts with ozone to form low-volatility products on the particle surfaces. Thus, the presence of PAHs in the gas phase during SOA formation could have significant effects on SOA formation growth kinetics, and possibly mass yields.

Fig. 9 through 11 show pairwise comparisons of the $d_m$ size distributions of pure SOA particles and those formed in the presence of a PAH. The data in these

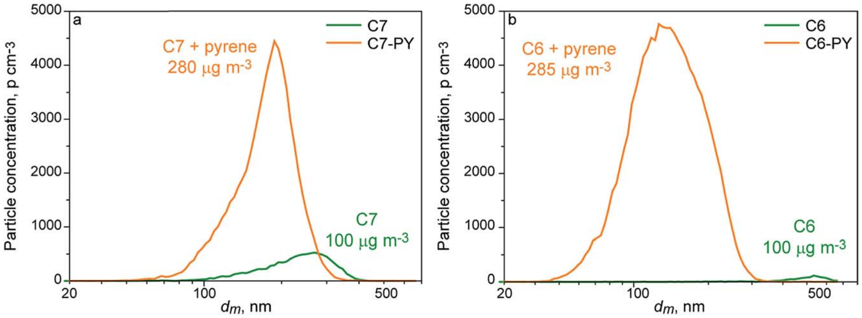

Fig. 9 (a) Mobility size distributions of 'pure' cycloheptene SOA particles (C7, green) and cycloheptene SOA particles formed in the presence of pyrene (C7-PY, orange); (b) mobility size distributions of 'pure' cyclohexene SOA particles (C6, green) and cyclohexene SOA particles formed in the presence of pyrene (C6-PY, orange).

plots correspond to the end of SOA formation (~2 hours after addition of ozone and SOA precursor), when changes in particle size become negligible. We start with a comparison of the $d_\mathrm{m}$ size distributions for C7-SOA and C7-PY-SOA, presented in Fig. 9a. It shows that the presence of pyrene during cycloheptene SOA formation leads to an increase in SOA loadings by a factor of nearly three (from 100 μg $\mathrm{m}^{-3}$ to 280 μg $\mathrm{m}^{-3}$), and in particle number concentrations by a factor of seven. Similarly, the formation of cyclohexene SOA is significantly enhanced in the presence of pyrene during SOA formation. Fig. 9b indicates an increase by a factor of nearly three in SOA loadings and an increase by more than a factor of 100 in particle number concentration.

To expand these results next we examine the impact of pyrene on the formation of α-pinene SOA. Fig. 10a and b show the comparisons of the $d_\mathrm{m}$ size distributions for αP-SOA and αP-PY-SOA, generated using 20 ppb and 5 ppb of α-pinene, respectively. The figures show that at higher (20 ppb) α-pinene concentration, the presence of pyrene results in an increase in SOA mass loadings by a factor of 1.7 and a small increase in particle number concentrations. However, for 5 ppb of α-pinene, the presence of pyrene leads to a fivefold increase in mass

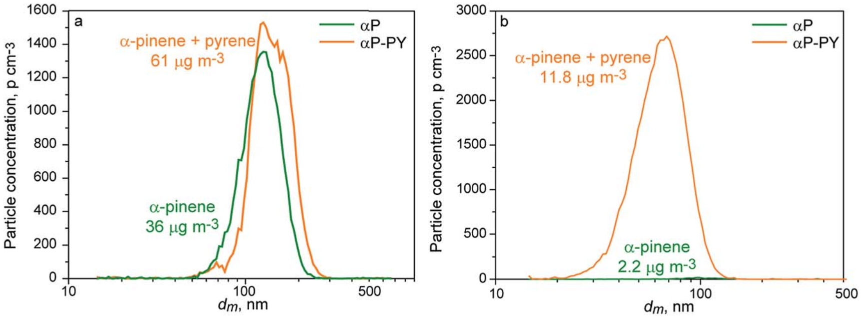

Fig. 10 (a) Mobility size distributions of SOA particles formed by ozonolysis of 20 ppb of α-pinene: pure (green) and formed in the presence of pyrene (orange); (b) mobility size distributions of SOA particles formed by ozonolysis of 5 ppb of α-pinene: pure (green) and formed in the presence of pyrene (orange).

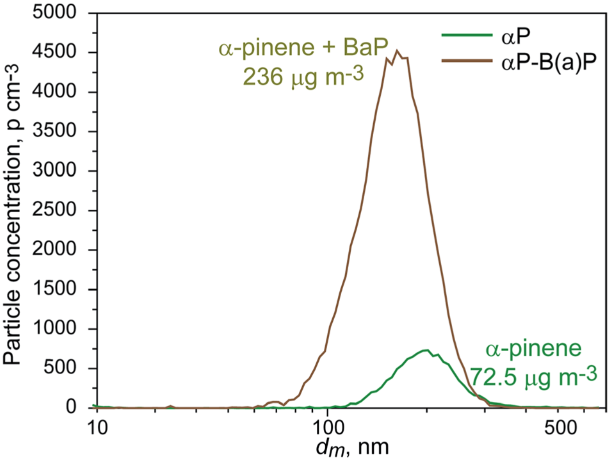

**Fig. 11** Mobility size distributions of 'pure' α-pinene SOA particles (green) and SOA particles formed in the presence of benzo(*a*)pyrene (BaP, brown).

loading (from 2.2 μg $m^{-3}$ for αP-SOA to 11.8 μg $m^{-3}$ for αP-PY-SOA) and a factor of 200 increase in the particle number concentrations.

The results of the formation studies presented in Fig. 10a and b suggest a simple pattern, in which the effect of pyrene on SOA loadings and particle number concentrations are directly related to the SOA formation and growth rates. When particle growth rate is reduced, *e.g.* at lower α-pinene concentrations, the effect of pyrene is more pronounced. Limonene SOA represents an extreme case, in which particle formation and growth rate is very high and the presence of pyrene barely affects the composition and evaporation kinetics of these SOA particles. Overall, the data seem to suggest competing processes of the PAHs adsorbing to the particle surfaces and reacting with ozone, and oxidation products of the SOA precursor condensing on the same surfaces. If condensation is fast, relatively fewer PAH molecules adsorb and react with ozone, thus diminishing the effect of PAHs on SOA properties.

To connect the formation studies presented here with the evaporation and mass spectroscopic analysis, presented in Fig. 2a and 5, respectively, we note that the SOA loadings of αP-PY-SOA were 1.5 times higher than those for αP-SOA.

The effects on SOA formation are not limited to pyrene. In Fig. 11 we demonstrate the effect of benzo(*a*)pyrene on SOA formed using 50 ppb of α-pinene. These data show that, despite a fairly high α-pinene concentration, the presence of ~7 ppt of BaP during SOA formation, results in a five-fold increase in particle mass concentrations and a six-fold increase in particle number concentrations. Here again, the results provide evidence that, even when present at very low concentrations, PAHs affect SOA formation significantly.

## Conclusions

We presented experimental data that demonstrate the effect of PAHs on the formation and properties of SOA particles formed by ozonolysis in the presence of the gas-phase PAHs. For all PAHs and all SOA precursors, except limonene, we observe significant differences in particle mass loadings, number concentrations, evaporation kinetics, composition, and viscosity, when comparing 'pure' SOA particles and those formed in the presence of PAHs.

We present data for six SOA precursors and 7 PAHs, with mixing ratios ranging from 7 ppt to 90 ppm. All SOA particles, formed in the presence of PAHs, contain both trapped unreacted PAHs and products of heterogeneous reactions between PAHs and ozone. These particles significantly differ from 'pure' SOA particles produced from the same precursor, in many respects. They exhibit slower evaporation kinetics, have larger fractions of non-volatile components, and higher viscosities. When aged, the fraction of non-volatile components increases to ~80% of the particle volume.

While gas-phase reactions between PAHs and ozone are too slow to effect SOA formation and properties, PAHs on surfaces react with ozone at a rate sufficiently high to become important. The data presented here show that when solid AS particles were introduced into a reaction chamber containing gas-phase pyrene and ozone, a reaction between ozone and pyrene ensued on the surface of the AS particles to produce a few nanometers thick organic layer, composed of pyrene oxidation products along with trapped unreacted pyrene molecules. In the evaporation chamber, this organic layer evaporated very slowly, reaching an asymptotic VFR of ~70% after 24 hours, at which point the evaporation rate becomes negligible. The data show that pyrene molecules, trapped in this layer, do not diffuse and evaporate faster than the pyrene oxidation products, indicating that the viscosity of the organic layer is significantly higher than that of α-pinene SOA at low RH ($>10^8$ Pa s).

The magnitude of the effects of PAHs on SOA formation observed here is surprisingly large. The presence of PAHs during SOA formation increases mass loadings by factors of two to five, and particle number concentrations, in some cases, by more than a factor of 100. The data suggest a simple relation between the magnitude of the PAHs effect on the SOA particles and the rate of SOA formation and growth, with the slower SOA formation and growth being more strongly affected by the PAHs.

Overall, higher mass loadings and particle number concentrations, lower evaporation rates, and hence increased lifetimes, compared to pure SOA from the same precursor, could significantly affect climate, weather, visibility, and human health. Furthermore, the increased viscosity and decreased volatility provides protection from further oxidation for trapped PAHs, thus increasing their lifetime in the atmosphere, enabling long-range transport of these toxic pollutants.[17,19]

These findings point to a synergistic relationship that exists between biogenic SOA and anthropogenic PAHs that represents a new mechanism for anthropogenic–biogenic interactions. The exact effect that PAHs have on SOA particles depends on many variables, such as the SOA precursors and their concentrations, the PAHs present and their concentrations, ozone concentration, and RH. The synergistic relationship presented here is clearly complex, requiring further research to develop a fundamental understanding of the processes involved and their atmospheric implications.

It is important to note that PAHs represent just one type of hydrophobic organics that can affect the properties of SOA particles. Similar effects were observed for dioctyl phthalate (DOP) and dioctyl sebacate (DOS), two plasticizers, whose concentrations in the experiments were 200 ppt and 20 ppt, respectively.[8]

α-Pinene SOA particles, formed in the presence of DOP or DOS, evaporated slower than pure αP-SOA and had an asymptotic VFR of ∼45%, which increased with aging to ∼60%.

Moreover, while the concentration of individual hydrophobic organics in the ambient atmosphere might not be at or near its equilibrium vapor pressure, many different hydrophobic organic molecules are simultaneously present in environments influenced by anthropogenic pollution. One must, therefore, consider the combined effect of all these compounds on the properties and formation of SOA particles that could alter the composition, loadings, and atmospheric lifetimes of both the SOA particles and the pollutants.

## Acknowledgements

This work was supported by the U. S. Department of Energy (DOE), Office of Science, Office of Basic Energy Sciences (BES), Division of Chemical Sciences, Geosciences and Biosciences. Additional support was provided by the DOE Atmospheric System Research (ASR) program (D. B.) and the Laboratory Directed Research and Development Program at Pacific Northwest National Laboratory (M. S.). Work by A. L. K. and S. L. M. S. was supported by the National Institutes of Health (NIH) – National Institute of Environmental Health Sciences (NIEHS) through grant number P42ES016465 and P30ES00210, and the National Science Foundation (NSF) through grant number AGS-11411214. Part of the research was performed using EMSL, a DOE Office of Science User Facility sponsored by the Office of Biological and Environmental Research and located at Pacific Northwest National Laboratory.

## References

1 J. E. Shilling, R. A. Zaveri, J. D. Fast, L. Kleinman, M. L. Alexander, M. R. Canagaratna, E. Fortner, J. M. Hubbe, J. T. Jayne, A. Sedlacek, A. Setyan, S. Springston, D. R. Worsnop and Q. Zhang, *Atmos. Chem. Phys.*, 2013, **13**, 2091–2113.

2 J. A. de Gouw, A. M. Middlebrook, C. Warneke, P. D. Goldan, W. C. Kuster, J. M. Roberts, F. C. Fehsenfeld, D. R. Worsnop, M. R. Canagaratna, A. A. P. Pszenny, W. C. Keene, M. Marchewka, S. B. Bertman and T. S. Bates, *J. Geophys. Res.: Atmos.*, 2005, **110**, D16305, DOI: 10.1029/2004JD005623.

3 R. Volkamer, J. L. Jimenez, F. San Martini, K. Dzepina, Q. Zhang, D. Salcedo, L. T. Molina, D. R. Worsnop and M. J. Molina, *Geophys. Res. Lett.*, 2006, **33**, L17811, DOI: 10.1029/2006GL026899.

4 A. H. Goldstein, C. D. Koven, C. L. Heald and I. Y. Fung, *Proc. Natl. Acad. Sci. U. S. A.*, 2009, **106**, 8835–8840.

5 D. V. Spracklen, J. L. Jimenez, K. S. Carslaw, D. R. Worsnop, M. J. Evans, G. W. Mann, Q. Zhang, M. R. Canagaratna, J. Allan, H. Coe, G. McFiggans, A. Rap and P. Forster, *Atmos. Chem. Phys.*, 2011, **11**, 12109–12136.

6 A. G. Carlton, R. W. Pinder, P. V. Bhave and G. A. Pouliot, *Environ. Sci. Technol.*, 2010, **44**, 3376–3380.

7 A. P. Bateman, Z. Gong, T. H. Harder, S. S. de Sá, B. Wang, P. Castillo, S. China, Y. Liu, R. E. O'Brien, B. Palm, H. W. Shiu, G. da Silva, R. Thalman, K. Adachi, M. L. Alexander, P. Artaxo, A. K. Bertram, P. R. Buseck, M. K. Gilles,

J. L. Jimenez, A. Laskin, A. O. Manzi, A. Sedlacek, R. A. F. Souza, J. Wang, R. Zaveri and S. T. Martin, *Atmos. Chem. Phys. Discuss.*, 2016, **2016**, 1–44.

8 T. D. Vaden, D. Imre, J. Beranek, M. Shrivastava and A. Zelenyuk, *Proc. Natl. Acad. Sci. U. S. A.*, 2011, **108**, 2190–2195.

9 WHO, *Health Risks of Persistent Organic Pollutants from Long-range Transboundary Air Pollution*, European Centre for Enviornment and Health, 2002.

10 R. Lohmann and G. Lammel, *Environ. Sci. Technol.*, 2004, **38**, 3793–3803.

11 R. W. MacDonald, L. A. Barrie, T. F. Bidleman, M. L. Diamond, D. J. Gregor, R. G. Semkin, W. M. J. Strachan, Y. F. Li, F. Wania, M. Alaee, L. B. Alexeeva, S. M. Backus, R. Bailey, J. M. Bewers, C. Gobeil, C. J. Halsall, T. Harner, J. T. Hoff, L. M. M. Jantunen, W. L. Lockhart, D. Mackay, D. C. G. Muir, J. Pudykiewicz, K. J. Reimer, J. N. Smith, G. A. Stern, W. H. Schroeder, R. Wagemann and M. B. Yunker, *Sci. Total Environ.*, 2000, **254**, 93–234.

12 T. Primbs, S. Simonich, D. Schmedding, G. Wilson, D. Jaffe, A. Takami, S. Kato, S. Hatakeyama and Y. Kajii, *Environ. Sci. Technol.*, 2007, **41**, 3551–3558.

13 T. Primbs, A. Piekarz, G. Wilson, D. Schmedding, C. Higginbotham, J. Field and S. M. Simonich, *Environ. Sci. Technol.*, 2008, **42**, 6385–6391.

14 S. A. Genualdi, R. K. Killin, J. Woods, G. Wilson, D. Schmedding and S. L. M. Simonich, *Environ. Sci. Technol.*, 2009, **43**, 1061–1066.

15 E. Galarneau, T. F. Bidleman and P. Blanchard, *Atmos. Environ.*, 2006, **40**, 182–197.

16 W. T. Wang, S. L. M. Simonich, W. Wang, B. Giri, J. Y. Zhao, M. A. Xue, J. Cao, X. X. Lu and S. Tao, *Atmos. Res.*, 2011, **99**, 197–206.

17 A. Zelenyuk, D. Imre, J. Beránek, E. Abramson, J. Wilson and M. Shrivastava, *Environ. Sci. Technol.*, 2012, **46**, 12459–12466.

18 E. Abramson, D. Imre, J. Beranek, J. Wilson and A. Zelenyuk, *Phys. Chem. Chem. Phys.*, 2013, **15**, 2983–2991.

19 M. Shrivastava, S. Lou, A. Zelenyuk, R. C. Easter, R. Corley, P. J. Rasch, J. Fast, S. Simonich and S. Tao, *Proc. Natl. Acad. Sci. U. S. A.*, 2017, **114**(6), 1246–1251, DOI: 10.1073/pnas.1618475114.

20 T. Berkemeier, S. S. Steimer, U. K. Krieger, T. Peter, U. Poschl, M. Ammann and M. Shiraiwa, *Phys. Chem. Chem. Phys.*, 2016, **18**, 12662–12674.

21 I. J. Keyte, R. M. Harrison and G. Lammel, *Chem. Soc. Rev.*, 2013, **42**, 9333–9391.

22 S. Gross and A. K. Bertram, *J. Phys. Chem. A*, 2008, **112**, 3104–3113.

23 J. Ringuet, A. Albinet, E. Leoz-Garziandia, H. Budzinski and E. Villenave, *Atmos. Environ.*, 2012, **61**, 15–22.

24 T. F. Kahan, N. O. A. Kwamena and D. J. Donaldson, *Atmos. Environ.*, 2006, **40**, 3448–3459.

25 N. O. A. Kwamena, J. A. Thornton and J. P. D. Abbatt, *J. Phys. Chem. A*, 2004, **108**, 11626–11634.

26 C. Liu, P. Zhang, B. Yang, Y. Wang and J. Shu, *Environ. Sci. Technol.*, 2012, **46**, 7575–7580.

27 U. Poschl, T. Letzel, C. Schauer and R. Niessner, *J. Phys. Chem. A*, 2001, **105**, 4029–4041.

28 S. Zhou, A. K. Y. Lee, R. D. McWhinney and J. P. D. Abbatt, *J. Phys. Chem. A*, 2012, **116**, 7050–7056.

29 S. Zhou, M. Shiraiwa, R. D. McWhinney, U. Poeschl and J. P. D. Abbatt, *Faraday Discuss.*, 2013, **165**, 391–406.

30 S. N. Chu, S. Sands, M. R. Tomasik, P. S. Lee and V. F. McNeill, *J. Am. Chem. Soc.*, 2010, **132**, 15968–15975.

31 J. J. Yao, Z. H. Huang and S. J. Masten, *Water Res.*, 1998, **32**, 3001–3012.

32 S. K. Gao, Y. Zhang, J. W. Meng and J. N. Shu, *Atmos. Environ.*, 2009, **43**, 3319–3325.

33 K. Miet, K. Le Menach, P. M. Flaud, H. Budzinski and E. Villenave, *Atmos. Environ.*, 2009, **43**, 3699–3707.

34 J. J. Yao, Z. H. Huang and S. J. Masten, *Water Res.*, 1998, **32**, 3235–3244.

35 M. Shiraiwa, Y. Sosedova, A. Rouvière, H. Yang, Y. Zhang, J. P. D. Abbatt, M. Ammann and U. Pöschl, *Nat. Chem.*, 2011, **3**, 291–295.

36 E. Gloaguen, E. R. Mysak, S. R. Leone, M. Ahmed and K. R. Wilson, *Int. J. Mass Spectrom.*, 2006, **258**, 74–85.

37 A. Zelenyuk, J. Yang, C. Song, R. A. Zaveri and D. Imre, *Environ. Sci. Technol.*, 2008, **42**, 8033–8038.

38 T. D. Vaden, C. Song, R. A. Zaveri, D. Imre and A. Zelenyuk, *Proc. Natl. Acad. Sci. U. S. A.*, 2010, **107**, 6658–6663.

39 A. Zelenyuk and D. Imre, *Int. Rev. Phys. Chem.*, 2009, **28**, 309–358.

40 A. Zelenyuk, J. Yang, C. Song, R. A. Zaveri and D. Imre, *J. Phys. Chem. A*, 2008, **112**, 669–677.

41 A. Zelenyuk, J. Yang, E. Choi and D. Imre, *Aerosol Sci. Technol.*, 2009, **43**, 411–424.

42 A. Zelenyuk, D. Imre, J. Wilson, Z. Zhang, J. Wang and K. Mueller, *J. Am. Soc. Mass Spectrom.*, 2015, **26**, 257–270.

43 A. Zelenyuk, J. Yang and D. Imre, *Int. J. Mass Spectrom.*, 2009, **282**, 6–12.

44 P. F. DeCarlo, J. R. Kimmel, A. Trimborn, M. J. Northway, J. T. Jayne, A. C. Aiken, M. Gonin, K. Fuhrer, T. Horvath, K. S. Docherty, D. R. Worsnop and J. L. Jimenez, *Anal. Chem.*, 2006, **78**, 8281–8289.

45 J. Wilson, D. Imre, J. Beranek, M. Shrivastava and A. Zelenyuk, *Environ. Sci. Technol.*, 2015, **49**, 243–249.

46 M. Shrivastava, A. Zelenyuk, D. Imre, R. Easter, J. Beranek, R. A. Zaveri and J. Fast, *J. Geophys. Res.: Atmos.*, 2013, **118**(8), 3328–3342, DOI: 10.1002/jgrd.50160.

47 E. J. Davis, P. Ravindran and A. K. Ray, *Chem. Eng. Commun.*, 1980, **5**, 251–268.

48 M. Ehn, J. A. Thornton, E. Kleist, M. Sipila, H. Junninen, I. Pullinen, M. Springer, F. Rubach, R. Tillmann, B. Lee, F. Lopez-Hilfiker, S. Andres, I.-H. Acir, M. Rissanen, T. Jokinen, S. Schobesberger, J. Kangasluoma, J. Kontkanen, T. Nieminen, T. Kurten, L. B. Nielsen, S. Jorgensen, H. G. Kjaergaard, M. Canagaratna, M. Dal Maso, T. Berndt, T. Petaja, A. Wahner, V.-M. Kerminen, M. Kulmala, D. R. Worsnop, J. Wildt and T. F. Mentel, *Nature*, 2014, **506**, 476–479.

49 T. Jokinen, T. Berndt, R. Makkonen, V.-M. Kerminen, H. Junninen, P. Paasonen, F. Stratmann, H. Herrmann, A. B. Guenther, D. R. Worsnop, M. Kulmala, M. Ehn and M. Sipila, *Proc. Natl. Acad. Sci. U. S. A.*, 2015, **112**, 7123–7128.

50 S. Gao, N. L. Ng, M. Keywood, V. Varutbangkul, R. Bahreini, A. Nenes, J. W. He, K. Y. Yoo, J. L. Beauchamp, R. P. Hodyss, R. C. Flagan and J. H. Seinfeld, *Environ. Sci. Technol.*, 2004, **38**, 6582–6589.

51 M. Kalberer, D. Paulsen, M. Sax, M. Steinbacher, J. Dommen, A. S. H. Prevot, R. Fisseha, E. Weingartner, V. Frankevich, R. Zenobi and U. Baltensperger, *Science*, 2004, **303**, 1659–1662.

52 M. P. Tolocka, M. Jang, J. M. Ginter, F. J. Cox, R. M. Kamens and M. V. Johnston, *Environ. Sci. Technol.*, 2004, **38**, 1428–1434.

53 P. J. Ziemann, *Int. Rev. Phys. Chem.*, 2011, **30**, 161–195.

54 C. D. Cappa and K. R. Wilson, *Atmos. Chem. Phys.*, 2011, **11**, 1895–1911.

55 K. R. Kolesar, Z. Li, K. R. Wilson and C. D. Cappa, *Environ. Sci. Technol.*, 2015, **49**, 12242–12252.

56 F. D. Lopez-Hilfiker, C. Mohr, E. L. D'Ambro, A. Lutz, T. P. Riedel, C. J. Gaston, S. Iyer, Z. Zhang, A. Gold, J. D. Surratt, B. H. Lee, T. Kurten, W. W. Hu, J. Jimenez, M. Hallquist and J. A. Thornton, *Environ. Sci. Technol.*, 2016, **50**, 2200–2209.

57 P. Roldin, A. C. Eriksson, E. Z. Nordin, E. Hermansson, D. Mogensen, A. Rusanen, M. Boy, E. Swietlicki, B. Svenningsson, A. Zelenyuk and J. Pagels, *Atmos. Chem. Phys.*, 2014, **14**, 7953–7993.

58 J. F. Widmann, C. M. Heusmann and E. J. Davis, *Colloid Polym. Sci.*, 1998, **276**, 197–205.

59 M. Riva, S. H. Budisulistiorini, Z. F. Zhang, A. Gold and J. D. Surratt, *Atmos. Environ.*, 2016, **130**, 5–13.

60 M. Riva, S. H. Budisulistiorini, Z. Zhang, A. Gold, J. A. Thornton, B. J. Turpin and J. D. Surratt, *Atmos. Environ.*, 2017, **152**, 314–322.

61 R. E. Cochran, H. Jeong, S. Haddadi, R. F. Derseh, A. Gowan, J. Beranek and A. Kubatova, *Atmos. Environ.*, 2016, **128**, 92–103.

62 R. E. Cochran, I. P. Smoliakova and A. Kubatova, *Int. J. Mass Spectrom.*, 2016, **397**, 6–17.

63 L. Renbaum-Wolff, J. W. Grayson, A. P. Bateman, M. Kuwata, M. Sellier, B. J. Murray, J. E. Shilling, S. T. Martin and A. K. Bertram, *Proc. Natl. Acad. Sci. U. S. A.*, 2013, **110**(20), 8014–8019, DOI: 10.1073/pnas.1219548110.

64 Y. J. Li, P. Liu, Z. Gong, Y. Wang, A. P. Bateman, C. Bergoend, A. K. Bertram and S. T. Martin, *Environ. Sci. Technol.*, 2015, **49**, 13264–13274.

65 E. Järvinen, K. Ignatius, L. Nichman, T. B. Kristensen, C. Fuchs, C. R. Hoyle, N. Höppel, J. C. Corbin, J. Craven, J. Duplissy, S. Ehrhart, I. El Haddad, C. Frege, H. Gordon, T. Jokinen, P. Kallinger, J. Kirkby, A. Kiselev, K. H. Naumann, T. Petäjä, T. Pinterich, A. S. H. Prevot, H. Saathoff, T. Schiebel, K. Sengupta, M. Simon, J. G. Slowik, J. Tröstl, A. Virtanen, P. Vochezer, S. Vogt, A. C. Wagner, R. Wagner, C. Williamson, P. M. Winkler, C. Yan, U. Baltensperger, N. M. Donahue, R. C. Flagan, M. Gallagher, A. Hansel, M. Kulmala, F. Stratmann, D. R. Worsnop, O. Möhler, T. Leisner and M. Schnaiter, *Atmos. Chem. Phys.*, 2016, **16**, 4423–4438.